SCIENTIFIC REPORTS

Correspondence and requests for materials should be addressed to M.H.K. (mhkim@ postech.ac.kr)

* These authors contributed equally to this work.

A Novel Role of Three Dimensional Graphene Foam to Prevent Heater Failure during Boiling

Ho Seon Ahn[1]*, Ji Min Kim[2]*, Chibeom Park[3], Ji-Wook Jang[4], Jae Sung Lee[5,4], Hyungdae Kim[6], Massoud Kaviany[5,7] & Moo Hwan Kim[5,2]

[1]Division of Mechanical System Engineering, Incheon National University, Incheon, Republic of Korea, [2]Department of Mechanical Engineering, POSTECH, Pohang, Republic of Korea, [3]Department of Chemistry, POSTECH, Pohang, Republic of Korea, [4]Department of Chemical Engineering, POSTECH, Pohang, Republic of Korea, [5]Division of Advanced Nuclear Engineering, POSTECH, Pohang, Republic of Korea, [6]Department of Nuclear Engineering, Kyung Hee University, Yong In, Republic of Korea, [7]Department of Mechanical Engineering, University of Michigan, Ann Arbor, USA.

We report a novel boiling heat transfer (NBHT) in reduced graphene oxide (RGO) suspended in water (RGO colloid) near critical heat flux (CHF), which is traditionally the dangerous limitation of nucleate boiling heat transfer because of heater failure. When the heat flux reaches the maximum value (CHF) in RGO colloid pool boiling, the wall temperature increases gradually and slowly with an almost constant heat flux, contrary to the rapid wall temperature increase found during water pool boiling. The gained time by NBHT would provide the safer margin of the heat transfer and the amazing impact on the thermal system as the first report of graphene application. In addition, the CHF and boiling heat transfer performance also increase. This novel boiling phenomenon can effectively prevent heater failure because of the role played by the self-assembled three-dimensional foam-like graphene network (SFG).

R ecently, there has been much interest in graphene, which is composed of a single layer of carbon atoms in a hexagonal lattice, because of its extreme electrical and thermal properties[1–6]. The lattice thermal conductivity of graphene has been studied by theoretical and experimental investigations; *e.g.*, the phonon thermal conductivity of single-layer graphene at room temperature is in the range of 2000–5000 W/m·K, depending on the flake width, defect concentration, and roughness of the edges[7]. This excellent thermal conductivity is very attractive for heat-transfer applications. However, studies of heat transfer applications using graphene have not yet been reported in the literature. Among the many heat transfer methods, phase-change heat transfer from liquid to vapor, known as boiling heat transfer, is the most efficient, since latent heat has a large capacity. Boiling heat transfer is used in nuclear power plants, electric chip cooling, air conditioners, and refrigerators. Boiling heat transfer is characterized by the heat flux (W·m^{-2}) and wall temperature (°C) of the heater surface during vapor bubble generation. However, there is a limitation for boiling heat transfer, called the maximum heat flux, boiling crisis, or critical heat flux (CHF, W·m^{-2}), which is a dangerous phenomenon in thermal systems. When CHF occurs, it occurs suddenly over a short time scale, and cannot be stopped. The wall temperature increases very rapidly because the vapor covers the entire heater surface, instantly blocking heat transfer and leading to failure of the heater material. The CHF phenomenon is complex, difficult to understand, irreversible, and unpredictable; thus, many studies have tried to predict CHF conditions for thermal systems to avoid encountering a dangerous situation. There have been many attempts to increase the CHF point for effective and safer heat transfer by using improved heater-surface wettability[8–12], nanofluids as the working fluid[13–16], and micro/nano-structured heater surfaces[17–20].

Here, we report a novel boiling heat transfer phenomenon when using reduced graphene oxide (RGO) suspended in water (RGO colloid), which is eliminated the sudden and rapid increase of wall temperature at CHF, and enhanced both CHF and boiling heat transfer (BHT). During boiling in the RGO colloid, a self-assembled three-dimensional (3D) interconnected foam-like graphene layer (SFG) and base graphene multi-layer (BGL) are formed on the heater surface. This induces the novel boiling heat transfer phenomenon (NBHT), providing assurance of a highly efficient and safe boiling heat transfer mode. The mechanisms for this phenom-enon are explained by examination of the heating method, and by conducting *ad-hoc* tests and a surface investigation, including high-speed visualization of the boiling phenomenon.
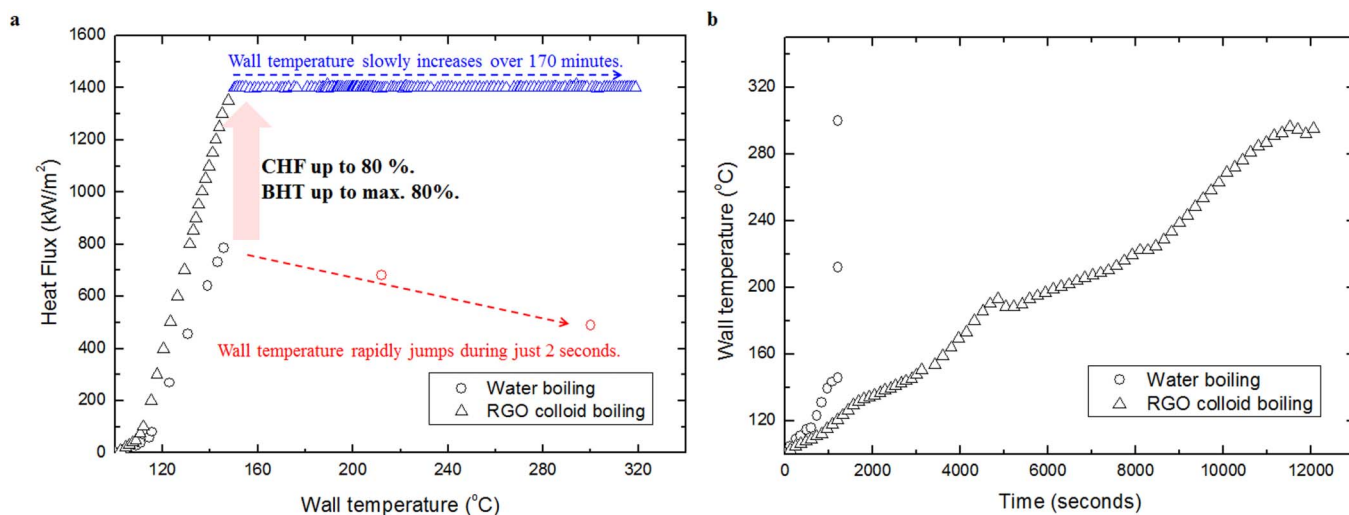
Figure 1 | Boiling characteristics of RGO colloid and time history of the heat flux and wall temperature on the SiO$_2$ heater. (a) Boiling curve, which is characterized by the heat flux and wall temperature, shows the water and RGO colloid boiling. At the maximum heat flux (CHF), the wall temperature in water boiling increases rapidly, however, it in RGO colloid boiling increases very slowly. (b) Wall temperature of RGO colloid boiling increases very slowly with time after heat flux reaches the CHF. The margin of time can provide the assurance of more effective and safer heat transfer condition near CHF.

Results

The 0.0005-wt% RGO colloid is prepared (Supplementary Fig. S1a). The RGO flakes are characterized by transmission electron microscopy (TEM) and atomic force microscopy (AFM) observations (Supplementary Fig. S1b, c, d). Over 90% of the RGO flakes are observed as a monolayer. The size of the suspended RGO flakes in water measured by AFM is 0.5–1.0 μm. A steady-state heat flux is applied on the heater surface (SiO$_2$ with a Pt-film heater) at 50- and 100-kW·m^{-2} increments at the saturated condition of atmospheric pressure (Supplementary Fig. S2, S3). During water boiling, CHF occurs at a heat flux of 800 kW·m^{-2} and a wall temperature of 150°C (Figure 1a). The wall temperature increases suddenly to 300°C within just 2 seconds. When the heat flux and wall temperature reach maximum heat flux (CHF) during boiling heat transfer, the heat transfer regime changes rapidly from nucleate boiling to film boiling, followed by CHF and the transition boiling regime (Supplementary Fig. S4). However, during RGO colloid boiling, the wall temperature starts to increase slowly at a heat flux of 1420 kW·m^{-2} and a wall temperature of 150°C. It takes nearly 170 minutes to reach a wall temperature of 320°C, eliminating the sudden temperature increase, which is found during water boiling. The time scale of the wall temperature increase at and after CHF differs significantly for water boiling and RGO colloid boiling (Figure 1b). The more interesting result is the 80% increase in both the CHF and BHT during the NBHT.

We first observe the NBHT and determine the reason for it through an investigation of the heater surface. SEM and optical microscopy observations of the heater surface indicates a porous layer of RGO flakes, known as a self-assembled three-dimensional foam-like graphene layer (SFG) (Fig. 2a). According to Ahn *et al.*[21], nucleate boiling in RGO colloid provides a base graphene multilayer (BGL) and an SFG sequentially as the heat flux increases (Fig. 2b). The BGL is formed in the heat flux range of 100–400 kW·m^{-2}. The RGO flakes are stacked neatly along the substrate by the movement of the triple line (liquid–vapor–solid) during bubble growth (Supplementary Fig. S5, S6). As the heat flux increases, more bubbles are generated faster, and these merge together, forming a large mushroom. The SFG is formed as a result of the merging of small bubbles by downward suppression at nucleation sites, and the pore size of SFG is strongly dependent with the heat flux; smaller pore size as higher heat flux[22]. The BGL and SFG are formed by nucleate boiling

can be represented by the simple schematic diagram, which is supported by side-view SEM observations (Fig. 2b). We investigate the alignment of the RGO flakes of the BGL and SFG through TEM and magnified SEM observations (Fig. 2c). The junction of the SFG also consisted of well-aligned RGO flakes. In addition, we confirm formation and effect of SFG on various substrates as heaters such as metal (copper) during the nucleate boiling in RGO colloid (Supplementary Fig. S7). In this case, we observe the same phenomenon at the maximum heat flux: the wall temperature increased slowly. In addition, we use an *ad-hoc* test to confirm the role of only the BGL and SFG. After pre-coating the copper heater with the SFG, followed by nucleate boiling with a heat flux of 1200 kW·m^{-2} in RGO colloid, the RGO colloid is removed from the pool chamber and the water is boiled. This validates that it was only the role of the BGL and SFG that eliminated the sudden wall temperature increase at the maximum heat flux, and only nucleate boiling in RGO colloid can form the BGL and SFG with pores that were 5–10 μm in size. The SFG is observed on the copper heater before and after the *ad-hoc* test (Supplementary Fig. S8). Thus, it is concluded that the SFG could be formed on various substrates and leads the NBHT. Next, we investigate the reason of the NBHT through the boiling visualization, because the relation among liquid, vapor, and surface affects strongly the boiling heat transfer and CHF. Since 0.0005-wt% RGO colloid is not transparent, the bubbles on the heater cannot be visualized. Thus, we visualized water boiling on an SFG-coated copper heater by using a high-speed camera at 1000 frames per second. Water boiling on the bare copper heater was visualized before, at, and after CHF (Fig. 3a). A thin macrolayer is formed beneath the large bubble mushroom at a heat flux of 1400 kW·m^{-2}. A dry patch, which is a large dry area on the surface due to imbalance of liquid supply and vaporization, is formed at the center of the heater surface beneath the bubble at a heat flux of 1504 kW·m^{-2} (CHF). The vapor film from the edge of the heater extends to the center of the heater and connected with the dry patch, so that finally the vapor film covers the entire heater surface. This suggests that the dry patch may play a role in the formation of a hot/dry spot just before CHF. Once the vapor covers the heater surface entirely, the surface temperature increases suddenly because of the thermal resistance of the vapor, since conduction heat transfer is not dominant through a vapor film[22,23]. Water boiling on the SFG-coated copper heater is also visualized during film boiling and during the novel boiling heat transfer phenomenon (Fig. 3b). A dry patch is
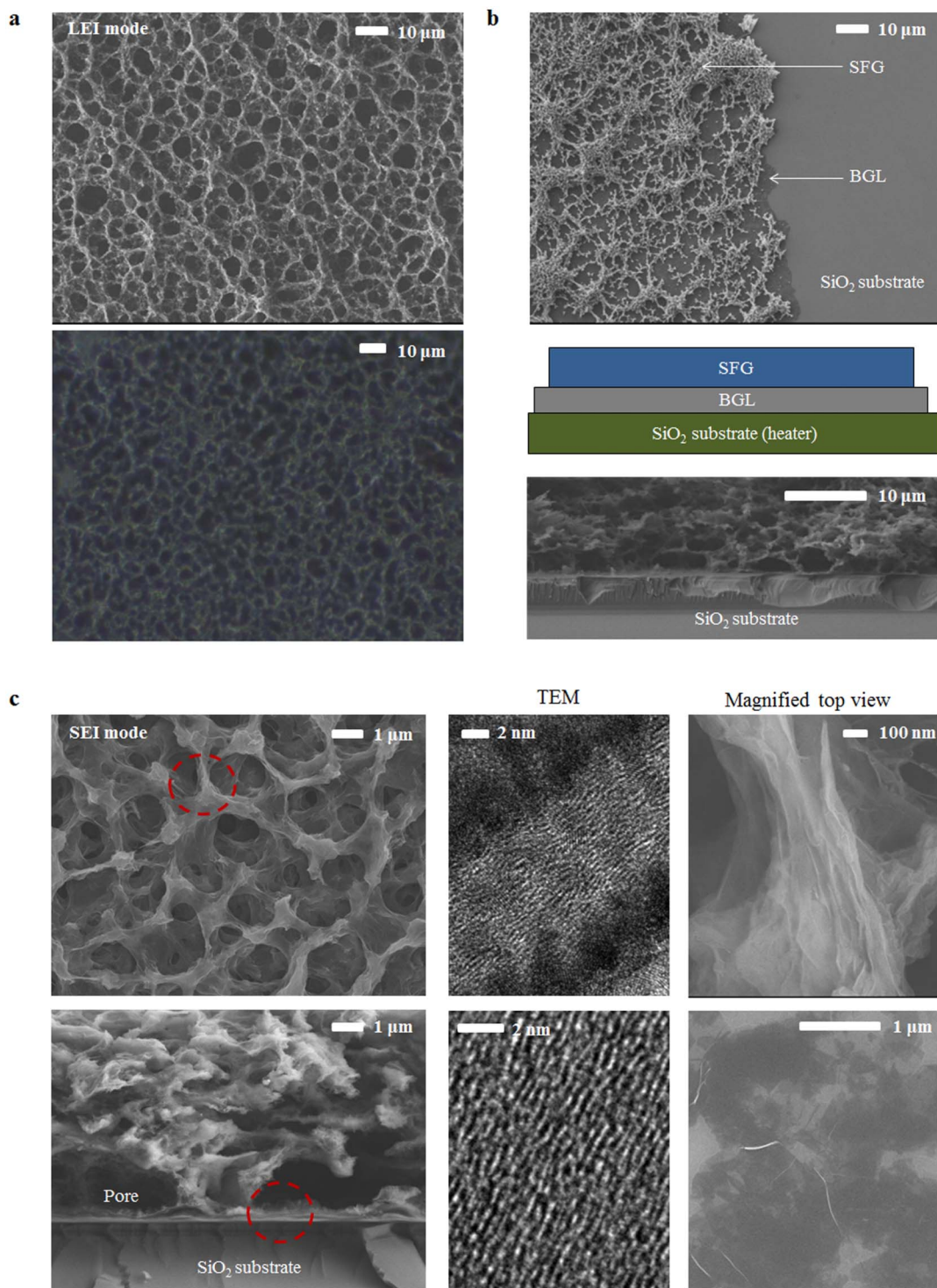
2

Figure 2 | Self-assembled three-dimensional foam-like graphene network (SFG) and Base graphene multi-layer (BGL) formation through nucleate boiling. (a) Scanning Electron Microscope (SEM) and optical magnified view of the SFG. After RGO colloid boiling, the surface characteristics of RGO coatings are investigated by SEM. (b) schematic diagram and side-view of the BGL and SFG (c) RGO flakes of the BGL and SFG are well aligned through the top-view and side-view of SEM, Transparent Electron Microscope (TEM) view at the junction of SFG and the side of BGL, and the magnified top-view of SEM.

observed when the wall temperature starts to increase slowly at a heat flux of 1700 kW·m^{-2}, but it does not grow larger, and nucleate boiling is maintained despite a wall temperature of 209°C.

Discussion

We suggest that the SFG serves two major roles: it spreads the heat of the SFG and BGL during nucleate boiling, and its saturated porous consistency with many micro-sized pores prevents CHF from being triggered. First, we consider how the BGL and SFG can spread the heat during nucleate boiling. The effective thermal conductivity of dry graphene foam was measured by Pettes et al.[24] and found to be much smaller than that of the dense layer that formed adjacent to the surface in our BGL beneath the SFG. Based on the results of Shin and Kaviany[25], it seems likely that the thermal conductivity interface
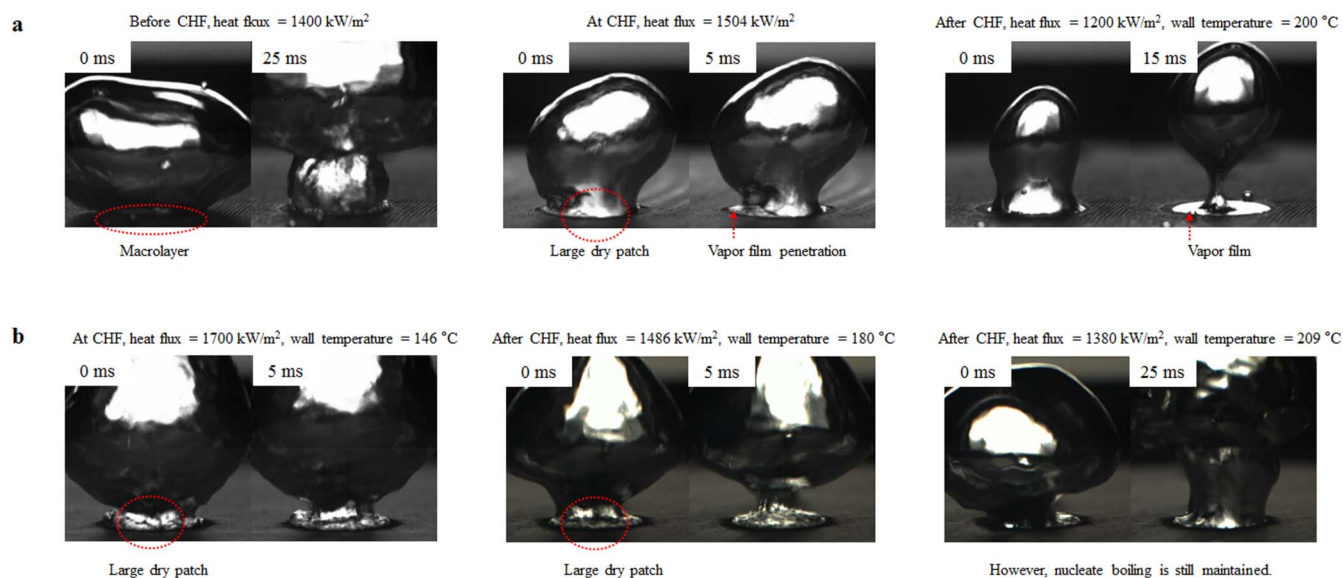
Figure 3 | Boiling visualization on clean and RGO flakes pre-coated copper heaters before, at, and after CHF. (a) Water boiling on a clean copper heater. Before CHF, a large mushroom of vapor is formed on an entire heater. At CHF, the large dry patch (spot) is observed in the large mushroom. At the edge of heater, the vapor film goes into the large dry path and meets with the large dry patch. Finally, the vapor film covers the entire heater. A film boiling is developed with the rapid wall temperature increase. (b) Water boiling on RGO flakes pre-coated copper heater. At the CHF, the wall temperature starts to increase slowly and the large dry patch can be observed in the large mushroom. Even though the wall temperature reaches to 209°C, the nucleate boiling is still maintained with the large dry patch in the large mushroom, contrary to the film boiling development in water boiling on a clean copper heater.

between the graphene flakes in the foam and in the BGL is controlled by forces stronger than van der Waals forces (*e.g.*, covalent bonds). Therefore, the BGL should have an effective thermal conductivity that is one or two orders of magnitude higher than that of the graphene foam. According to Jang *et al.*[26], the estimated thermal conductivity of the graphene multilayer is 110–1100 $W \cdot K^{-1} \cdot m^{-1}$, depending on its thickness. As a graphene multilayer on a silicon substrate increases in thickness from 1–100 nm, its thermal conductivity increases. In the present study, the effective thermal conductivity of the 50- to 100-nm-thick BGL is thought to be at least one order of magnitude higher than that of the SiO_2 substrate. Thus, the BGL beneath the SFG can spread the heat, thereby preventing the dry patch from increasing in size.

Second, we consider how the BGL and SFG prevent CHF from being triggered due to its saturated porous consistency with many micro-sized pores. Fukusako *et al.*[27] described transition and film boiling on a liquid-saturated porous bed. They plotted the boiling curve for a porous medium without CHF; neither the wall temperature nor heat flux could maintain a steady state and both gradually increased. They postulated that transition boiling with a nucleate and film boiling consists of a wetted surface and vapor film conditions. The boiling characteristics show a gradual increase with time. However, the conditions were not the same as those of the present study, which included a zero superheat at the onset of nucleate boiling (ONB) and transition boiling starting at a low heat flux. Transition boiling on the porous medium could be the reason for the phenomenon observed in the present study, although our porous medium was in a saturated-liquid condition. In addition, Dhir and Liaw[28] proposed a unified analytical model of nucleate and transition pool boiling. CHF, nucleate boiling, and film boiling are determined by the vapor (dry) and liquid (wet) fraction, which can be the same regardless of whether the liquid is able to wet the heater surface. They postulated that transition boiling may be unified by the fraction of nucleate boiling versus film boiling. This means that our observed boiling phenomenon in RGO colloid can be explained by the larger contribution of nucleate boiling during transition boiling, which delays the transition of the boiling regime. This can also support

the nucleate boiling that is observed at a wall temperature of 300°C (Fig. 3b). Finally, Berenson[29] postulated that the roughness (peak to peak) of the heater surface influences transition boiling, when the nucleate boiling transitions into film boiling after reaching CHF. Transition boiling is a combination of unstable film boiling and unstable nucleate boiling existing alternately at any given location on the heater surface. The roughness provides the liquid a chance to meet the solid heater surface because of the instability of the vapor film. The measured roughness of the SFG was 5.9–10.5 μm, which was more than that of the SO_2 (2 nm)/copper heater (212 nm) surface (Supplementary Fig. S9). Recently, Kwark et al[16] reported that the nanofluids boiling should be defined as the transient state, because the nanoparticles are deposited more as the boiling time increasing. They showed that the wall temperature increases slowly with the constant heat flux and increasing the boiling time, because the nanoparticles coating layer is thicker and plays a role with the thermal resistance. Thus, we tried to conduct and compare the alumina-nanofluids boiling with RGO colloid boiling. In alumina-nanofluid with 0.001 wt.% (same with RGO colloid concentration), there is no transient boiling. (Supplementary Fig. 10) In RGO colloid boiling, there is a transient boiling as similar with the previously reported result by Kwark et al.[16], however, completely different with NBHT, because the time scale of increasing the wall temperature and the given condition such as the heat flux are different. In alumina-nanofluids boiling with higher concentration of 0.01 wt.%, there is a transient boiling. Thus, we could conclude that the NBHT near the CHF is a different phenomenon with the transient state.

Next, we investigate why the CHF in RGO colloid boiling increases compared to that of water boiling on a bare heater. A BGL is formed at a low heat flux, suggesting that the maximum heat flux might be determined by the role of the BGL. Even though an SFG is formed at a high heat flux, the BGL still remains at the bottom of the graphene structure (Supplementary Fig. S5, S6). First, the enhancement of thermal conductivity by the BGL may increase the CHF, affecting the thermal activity[30], which as a function of thermal conductivity, thermal capacity, density, and thickness of the heater surface material could affect the CHF as follows[31]:

$$S = \delta\sqrt{\rho_h c_h k_h} \qquad (1)$$

where S, δ, ρ_h, c_h, and k_h are the thermal activity, heater characteristic dimension, density, specific heat, and thermal conductivity of the heater material, respectively. The much-improved thermal activity (S) resulting from the BGL compared to that on the SiO$_2$ substrate can increase the CHF by delaying the formation and growth of the hot/dry spot[31]. Near CHF, depletion of the liquid under the large bubble mushroom leads to the creation of local dry spots, where temperatures rise rapidly under the influence of the imposed heat flux. The rate of this rise in temperature is moderated by the ability of the underlying structure to locally absorb and/or conduct heat to parts of the heater that are still experiencing nucleate boiling. If the heater is very thin or has poor thermal properties, CHF occurs soon after the formation of dry spots on the heater surface. However, if the heater is thick and has good thermal properties, the heater successfully absorbs and conducts heat away from local dry spots, thus keeping the dry-spot temperature from exceeding the critical re-wet temperature. For such high S, the heater may be able to sustain the sequential formation and extinction of many dry spots, relying on subsequent re-wetting of the surface to locally cool the surface back to the nucleate boiling regime[31]. This mechanism of high S can also explain the NBHT.

Second, we investigate the surface wettability of the BGL and SFG, which are hydrophobic and hydrophilic, respectively (Supplementary Fig. S11). Kandlikar[32] developed a CHF model with surface wettability; improved surface wettability increased CHF as follows:

$$q''_{CHF} = h_{fg}\rho_g^{1/2}\left(\frac{1+\cos\beta}{16}\right)\left[\frac{2}{\pi} + \frac{\pi}{4}(1+\cos\beta)\cos\varphi\right]^{1/2}$$
$$\left[\sigma g\left(\rho_l - \rho_g\right)\right]^{1/4} \qquad (2)$$

where β, ϕ, h_{fg}, ρ_l, ρ_g, σ, and g are the contact angle of the substrate, the oriented angle, the latent heat, the density of the liquid, the density of the gas, the surface tension, and the force of gravity, respectively. The enhanced wettability of the BGL can explain the increase in the CHF during RGO colloid boiling. Since the BGL is formed at the bottom of the stacked RGO layers, the water should

contact the hydrophobic SFG. However, the hydrophobic SFG works against increasing the maximum heat flux (Supplementary Fig. S12). This implies that the wettability is not sufficient to explain the CHF enhancement during RGO colloid boiling. During contact angle measurements, however, we find that water can be absorbed into the BGL and SFG. Even though graphene is a hydrophobic material in nature, the carboxyl group (–COOH) on the surface of the RGO flakes (Supplementary Fig. S13) may play a hydrophilic role. The water absorption of the BGL is faster than that of the SFG because the carboxyl group is partially more folded. During water absorption into the BGL and SFG, the contact angle at the triple point became smaller. This indicates that the BGL and SFG play a role with the porous medium, which can be saturated by water. As the wet area increasing, the water (liquid) has more chance to contact the liquid between the pores of the porous medium. Water absorption into the BGL and SFG can explain CHF enhancement, by supplementing liquid via capillary flow[14,16,17]. According to Kaviany[33], the vapor thickness (δ_g) and the two-phase length (δ_{gl}) of a porous medium are the main parameters that determine the CHF during boiling on a liquid-saturated porous medium (Supplementary Fig. S14). He showed that δ_{gl} tends to infinity when the forces of viscosity and gravity exactly balance. Then, the capillary pressure and saturation gradients in the porous medium become zero and finally CHF occurs. This means that the balance between drag and capillary forces in the liquid-saturated porous medium of the BGL and SFG may affect CHF enhancement. In addition, according to Liter and Kaviany[34], CHF can increase to five times the viscous-drag liquid choking limit. It seems reasonable to suggest that the CHF enhancement on the BGL and SFG layers provided by RGO colloid boiling is the result of improved surface wettability, the dynamics of the contact angle during water absorption, and the liquid-saturated porous medium following water absorption into the BGL and SFG. We use an environmental scanning electron microscope (E-SEM) for further investigation of the SFG water absorption phenomenon. At 7.5 mbar and 10°C with 100% humidity, heterogeneous condensation from the environment forms water droplets by cooling process into 1°C (Fig. 4a). With time, the water droplets are absorbed into the pores of the SFG, as shown in the dotted red circle (Fig. 4a). Then, a water droplet starts to regrow on the wetted pore. Here, we reverse the
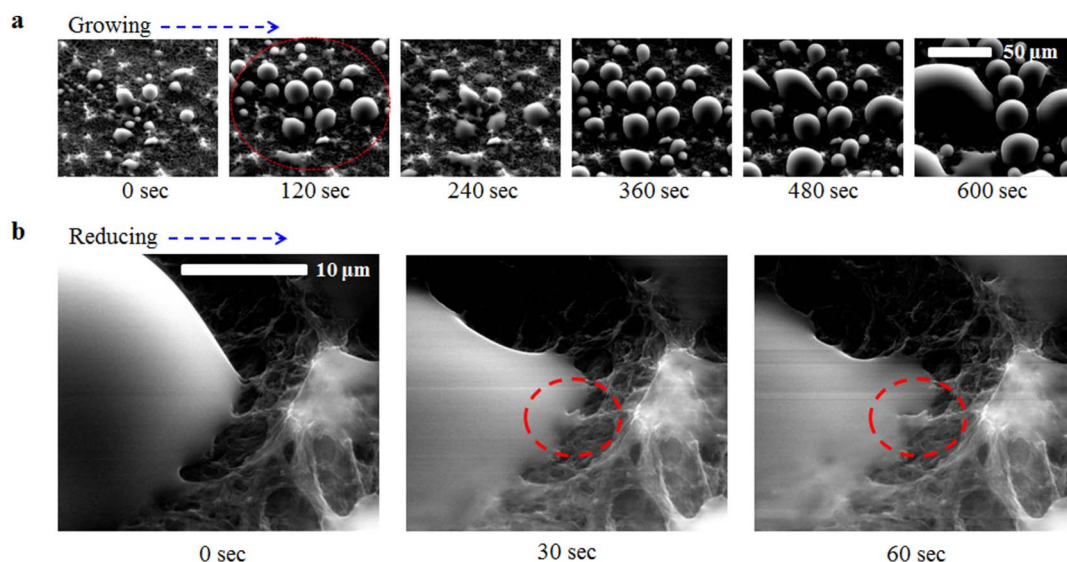

Figure 4 | Water absorption phenomenon on the BGL and SFG. (a) Environmental Scanning Electron Microscope (E-SEM) observation of water absorption on the SFG. In the initial stage, there are many small water droplets generated environmentally. As the water droplet growing with time, the lots water droplets in the red-dot circle are absorbed into the SFG. (b) Water droplet at the interface between a water droplet and the junction of the SFG. As the water droplet reducing with time, the wetted junction of the SFG can be observed in the red-dot circle. This triple line movement shows pinning characteristics and it means the wetted junction exhibits hydrophilic property.

condition to observe the triple line behavior in evaporation process. We highlight the interface between the water droplet and the SFG pore, where a curved water interface formed at the junction of the SFG, showing hydrophilic characteristics (Fig. 4b). We postulate that the carboxyl groups on the SFG structure are activated by contact with water so that it makes the surface to be hydrophilic and the triple line to advance slowly, resulting in water absorption phenomena. The wetted SFG interface may explain the water absorption into the SFG, supporting the increase in the maximum heat flux by liquid absorption[35]. In addition, the water absorption and the wetted junction of the SFG provide strong evidence for the role of the liquid-saturated porous medium in the transition boiling of our observed the NBHT.

Methods

RGO colloid preparation. The RGO colloid was synthesized from natural graphite powder using a two-step chemical process: first, the graphite oxide was produced from graphite powder using a modified Hummers method; and second, the RGO colloid was formed from the graphene oxide (GO) colloid[36–38]. The first step was an oxidation process of the graphite[36,37]. Two grams of graphite (<45 μm, Aldrich) and 1 g of sodium nitrate (Aldrich) were mixed with 50 ml of sulfuric acid (ACS 95–98%, Alfa Aesar) at low temperature (<10°C). Vigorous stirring was maintained to ensure reactions in all experiments. Six grams of potassium permanganate (Aldrich) were added, and the solution was allowed to react at low temperature for 30 min, followed by 2 h at 35°C. Then, 100 ml of distilled water (DI water) were added very slowly for 10 min, and the solution was allowed to react further at less than 95°C for 30 min to give a brown solution, the graphite oxide. The solution was mixed with 40 ml of hydrogen peroxide solution (36 ml of DI water + hydrogen peroxide solution (30 wt%, Aldrich)), and a membrane filtration process was applied twice to remove residual salts and acids. After filtration, the graphite oxide cake was freeze-dried to keep it in powder form for convenience. The second step was the reduction process of the graphene oxide (GO) colloid with hydrazine[38]. First, 0.25 g of the synthesized graphite oxide powder were suspended in 500 ml of DI water to give 0.05-wt% dispersion. The graphite oxide was exfoliated by ultrasonication (Fisher Scientific Sonic Dismembrator, Model 500, 400 W, 20 kHz, 30% amplitude) for 1 h to prepare the GO colloid. The colloid was mixed with 3.5 μl of ammonia solution (28–30 wt%, Samchun) and 0.5 μl of hydrazine solution (35 wt%, Aldrich) at 95°C for 1 h; the colloid turned from brown to black, the RGO colloid. The ammonia was used to control pH for stable dispersion of the RGO flakes in the colloid.

Pool-boiling experiment. The pool boiling experimental apparatus consisted of a boiling pool and a test heater (S2, S7). First of all, the boiling pool was a rectangular aluminum vessel having visualization window of polycarbonate. The volume was about 4 L and the water inside was heated and maintained at saturated condition by an emerged cartridge heater installed on the side wall. In the boiling experiments, the water level was maintained from vaporization by a reflux condenser on the top of the pool. The condenser was opened to atmosphere, so that the inside of pool could be maintained at saturation condition in atmospheric pressure. Next, we used two types of test heater; the silicon heater and the copper heater. Their specific characteristics are explained as following.

The silicon heater in the experiment was a 25 mm × 20 mm × 0.475-mm silicon wafer. The sidewall was insulated with polyether-ether-ketone (PEEK). The surface was mirror-polished, and on its opposite (bottom) side, a 15 mm × 10-mm platinum (Pt) pattern was deposited for joule heating. Four wires were connected to the Pt pattern to supply power and measure the voltage. A reference resistance was employed in series in the power circuit to measure the current, and its temperature was maintained at 10°C by a constant-temperature bath (JEIO TECH). The applied heat flux was calculated from the voltage and current at the heating area of the Pt pattern, as follows:

$$q'' = \frac{V \cdot I}{A}$$

The wall temperature was measured from the resistance of the Pt pattern; this was calibrated between 100 and 150°C. Before the boiling experiment, the working fluid was heated by a cartridge heater, which was immersed in the pool for 2 h for degassing. In the experiment, the heat flux was applied to the silicon heater by an alternating current (AC) power supply (120 V, 8.5 A) and increased to 100 kW/m² after 2 min for steady-state data gathering. Starting at 100 kW/m², the heat flux was increased in 10-kW/m² steps to observe the ONB. When the CHF occurred, the heat flux was maintained, and the novel boiling heat transfer phenomenon was observed. The copper heater in the experiment was a 10-mm-diameter cylindrical high-grade copper (99.999%) block. The sidewall was insulated with PEEK, similar to the silicon heater. The wall temperature was measured by a thermocouple inserted in the center of the copper block near the surface. The heat was transferred by conduction from a heating section with 5 kW of power; the heat section consisted of the conducting copper block and ten cartridge heaters with an individual maximum power of 500 W. The bottom of the copper heater cylinder was in contact with the heated section, and changes in the contact resistance between the two due to thermal expansion were

prevented by a spring system under the heated section. The applied heat flux was calculated as follows:

$$q'' = k\frac{\Delta T}{\Delta x}$$

where k is the conductivity of copper, ΔT the difference in the center temperature data near the contact in the heated section, and Δx is the distance from the temperature measuring point, 7 mm. Similar to the case of the silicon heater, the working fluid was heated by a cartridge heater that was immersed in the pool for 2 h for degassing before the boiling experiment. In the experiment, the heat flux was applied to the copper heater by contact with the heated section, and the rate of heat generation in the heated section was controlled by a silicon-controlled rectifier (SCR) unit (IPM3 9900 M). The response to control was slow due to the heat capacity of the heated section, so the heat flux could be increased continuously by assuming a quasi-steady state. When CHF occurred, the input condition to the SCR unit was maintained to observe the novel boiling heat transfer phenomenon.

High-speed visualization. A visualization technique using a high-speed camera was adopted to observe the novel boiling heat transfer phenomenon on the SFG pre-coated copper surface and to compare it with the CHF phenomenon on a bare copper surface. The pre-trigger function of the high-speed camera (Redlake MotionXtra HG-100K) was suitable for taking images of the CHF phenomenon. A 1000-W incandescent light source was installed opposite the camera to provide backlighting for the high-speed images. The images were focused on the heater surface and the tails of the bubble coalescences, and shot at a rate of 1000 frames per second.

Characterization. A high-resolution FE-SEM (JEOL JSM-7401F) was used to observe the geometrical characteristics of the RGO flake layer that coated the surface. Front and side view images of the surface were obtained at various magnifications from 500× to 50000× in LEI and SEI modes. The electrons were accelerated with 5 kV, 20 μA, under less than 1 mPa of pressure, and the resolution was 1 nm. The high-resolution [S]TEM (JOEL JEM-2200FS, with image Cs-corrector) was used to analyze the deposition pattern of RGO flakes in the BGL and SFG structures formed by nucleate boiling. Unlike the SEM analysis, a 100-nm-thick sample was prepared for the TEM analysis by a focused ion beam (FIB) (Helios, Pegasus). First, the RGO-coated surface was coated with 200 nm of titanium by electron (E)-beam deposition to prevent damage from the FIB process. Then, the sample was sliced and lifted up in the perpendicular direction to a 1-nm thickness using the FIB. The TEM images were obtained with up to 1,000,000× magnification. The electrons were accelerated with 200 keV, and the resolution was 0.1 nm. The E-SEM (Quanta200) was used to investigate the water absorption phenomenon on the BGL and SFG structured surface. Front and tilted views of the surface were observed with 1000× and 5000× magnifications. The phenomenon was observed by controlling the condensation process. Initially, the specimen was at steady state under saturated conditions (100% humidity) at 7.5 mbar and 10°C. Then, the condensation process was induced by rapidly cooling the specimen from 10°C to 1°C. Droplet growth and the water absorption phenomenon were observed during the condensation process. The electron was accelerated with 25 kV, 5 μA, under E-SEM mode, and the resolution was 1.5 nm. The detailed morphology and specimen height were investigated using AFM (Nanoscope IIIa, Digital Instrument Inc.) and Raman spectra were acquired using a commercial Raman spectroscope (Alpha 300R, WITEC) equipped with a 532-nm diode laser. Both the AFM and Raman studies were conducted at the Nanoscale Materials Research Laboratory at POSTECH. The contact angle was measured using a digital single-lens reflex (DSLR) camera (Nikon D7000). A 1-μl sessile DI water droplet on the BGL and SFG structure was observed under natural light and room temperature/atmospheric pressure conditions. The observations were continued until the droplet completely dried out. The bonding state and work function of each film were investigated using X-ray photoemission spectroscopy (XPS). The resistivity of each film was measured by the four-point probe method (Keithley Model 2000).

1. Novoselov, K. S. *et al.* Electric field effect in atomically thin carbon films. *Science* **306**, 666–669 (2004).
2. Geim, A. K. & Novoselov, K. S. The rise of graphene. *Nature Mat.* **6**, 183–191 (2007).
3. Balandin, A. A. *et al.* Superior thermal conductivity of single-layer graphene. *Nano Lett.* **8**, 902–907 (2008).
4. Kuzmenko, A. B., van Heumen, E., Carbone, F. & van der Marel, D. Universal optical conductance of graphite. *Phys. Rev. Lett.* **100**, 117401 (2008).
5. Stoller, M. D., Park, S., Zhu, Y., An, J. & Ruoff, R. S. Graphene-based ultracapacitors. *Nano Lett.* **8**, 3498–3502 (2008).
6. Niyogi, S. *et al.* Solution properties of graphite and graphene. *J. Am. Chem. Soc.* **128**, 7720–7721 (2006).
7. Balandin, A. A. *et al.* Superior thermal conductivity of single-layer graphene. *Nano Lett.* **8**, 902–907 (2008).
8. Liaw, S. P. & Dhir, V. K. Effect of surface wettability on transition boiling heat transfer from a vertical surface. *Proc. 8th Int. Heat Transfer Conf.* San Fransisco, CA, USA, **4**, 2031–2036 (1986).
9. Hahne, E. & Diesselhorst, T. Hydrodynamic and surface effects on the peak heat flux in pool boiling. *Proc. 6th Int. Heat Transfer Conf.* Toronto, Ontario, Canada, **1**, 209–219 (1978).

10. Maracy, M. & Winterton, R. H. S. Hysteresis and contact angle effects in transition pool boiling of water. *Int. J. Heat and Mass Transfer* **31**, 1433–1449 (1988).

11. Jeong, Y. H., Chang, W. J. & Chang, S. H. Wettability of heated surfaces under pool boiling using surfactant solutions and nano-fluids. *Int. J. Heat and Mass Transfer* **51**, 3025–3031 (2008).

12. Coursey, J. S. & Kim, J. Nanofluid boiling: The effect of surface wettability. *Int. J. Heat and Fluid Flow* **29**, 1577–1585 (2008).

13. Kim, H., Kim, J. & Kim, M. H. Effect of nanoparticles on CHF enhancement in pool boiling of nano-fluids. *Int. J. Heat and Mass Transfer* **49**, 5070–5074 (2006).

14. Kim, H. & Kim, M. H. Effect of nanoparticle deposition on capillary wicking that influences the critical heat flux in nanofluids. *App. Phys. Lett.* **91**, 014104 (2007).

15. Kim, S. J., Bang, I. C., Buongiorno, J. & Hu, L. W. Effects of nanoparticle deposition on surface wettability influencing boiling heat transfer in nanofluids. *App. Phys. Lett.* **89**, 153107 (2006).

16. Kwark, S. M., Kumar, R., Moreno, G., Yoo, J. & You, S. M. Pool boiling characteristics of low concentration nanofluids. *Int. J. Heat and Mass Transfer* **53**, 972–981 (2010).

17. Ahn, H. S., Jo, H. J., Kang, S. H. & Kim, M. H. Effect of liquid spreading due to nano/microstructures on the critical heat flux during pool boiling. *App. Phys. Lett.* **98**, 071908 (2011).

18. Chen, R. *et al*. Nanowires for enhanced boiling heat transfer. *Nano Lett.* **9**, 548–553 (2009).

19. Chu, K.-H., Enright, R. & Evelyn, N. W. Structured surfaces for enhanced pool boiling heat transfer. *App. Phys. Lett.* **100**, 241603 (2012).

20. Li, C. *et al*. Nanostructured copper interfaces for enhanced boiling. *Small* **4**, 1084 (2008).

21. Ahn, H. S. *et al*. Self-assembled foam-like graphene networks formed through nucleate boiling. *Sci. Rep.* **3**, 1396 (2013).

22. Ahn, H. S. *et al*. Controllable Pore Size of Three Dimensional Self-assembled Foam-like Graphene and its Wettability. *Carbon*, submitted.

23. Ahn, H. S. & Kim, M. H. Visualization study of critical heat flux mechanism on a small and horizontal copper heater. *Int. J. Multiphase Flow* **41**, 1–12 (2012).

24. Pettes, M. T., Ji, H., Ruoff, R. S. & Shi, L.Thermal transport in three-dimensional foam architectures of few-layer graphene nd ultrathin graphite. *Nano Lett.* **12**, 2959–5964 (2012).

25. Shin, S. & Kaviany, M. Interflake thermal conductance of edge-passivated graphene. *Phy. Rev. B* **84**, 235433 (2011).

26. Jang, W., Chen, Z., Bao, W., Lau, C. N. & Dames, C. Thickness-dependent thermal conductivity of encased graphene and ultrathin graphite. *Nano Lett.* **10**, 3909–3913 (2010).

27. Fukusako, S., Komoriya, T. & Seki, N. An experimental study of transition and film boiling heat transfer in liquid-saturated porous bed. *ASME J. Heat Transfer* **108**, 117–124 (1986).

28. Dhir, V. K. & Liaw, S. P. Framework for a unified model for nucleate and transition pool boiling. *ASME J. Heat Transfer* **111**, 739–746 (1989).

29. Berenson, P. J. Experiments on pool-boiling heat transfer. *Int. J. Heat Mass Transfer* **5**, 985–999 (1962).

30. Arik, M. & Bar-Cohen, A. Effusivity-based correlation of surface property effects in pool boiling CHF of dielectric liquid. *Int. J. Heat Mass Transfer* **46**, 3755–3765 (2003).

31. Arik, M, Bar-Cohen, A. & You, S. M. Enhancement of pool boiling critical heat flux in dielectric liquid by microporous coating. *Int. J. Heat Mass Transfer* **50**, 997–1009 (2007).

32. Kandlikar, S. G. A theoretical model to predict pool boiling CHF incorporating effects of contact angle and orientation. *ASME J. Heat Transfer* **123**, 1071–1079 (2001).

33. Kaviany, M. *Principles of Heat Transfer in Porous Media.* Springer–Verlag, New York, 582–585 (1991).

34. Liter, S. G. & Kaviany, M. Pool-boiling CHF enhancement by modulated porous-layer coating: Theory and experiment. *Int. J. Heat Mass Transfer* **44**, 4287–4311 (2001).

35. Ahn, H. S., Park, G., Kim, J. M., Kim, J. & Kim, M. H. The effect of water absorption on critical heat flux enhancement during pool boiling. *Exp. Therm. Fluid & Sci.* **42**, 187–195 (2012).

36. Kovtyukhova, N. I. *et al*. Layer-by-layer assembly of ultrathin composite films from micron-sized graphite oxide sheets and polycations. *Chem. Mater.* **11**, 771–778 (1999).

37. Hummers, W. S. & Offeman, R. E. Preparation of graphite oxide. *J. Am. Chem. Soc.* **80**, 1339 (1958).

38. Li, D., Müller, M. B., Gilje, S., Kaner, R. B. & Wallace, G. G. Processable aqueous dispersions of graphene nanosheets. *Nat. Nanotech.* **3**, 101–105 (2008).

Acknowledgements

Author contributions

H.S.A. designed the experiments and wrote the paper. J.M.K. performed the experiments and wrote the paper. C.P. helped obtain Raman and AFM data. J.-W.J. and J.S.L. helped to design the experiments. H.K. helped to write the manuscript and provided the evidence of SFG formation mechanism. M.K. advised the thermal conductivity of BGL and SFG. M.H.K. directed the research project. All authors discussed the results and contributed to the paper.

Additional information

Supplementary information accompanies this paper at http://www.nature.com/scientificreports

Competing financial interests: The authors declare no competing financial interests.

How to cite this article: Ahn, H.S. *et al*. A Novel Role of Three Dimensional Graphene Foam to Prevent Heater Failure during Boiling. *Sci. Rep.* **3**, 1960; DOI:10.1038/srep01960 (2013).